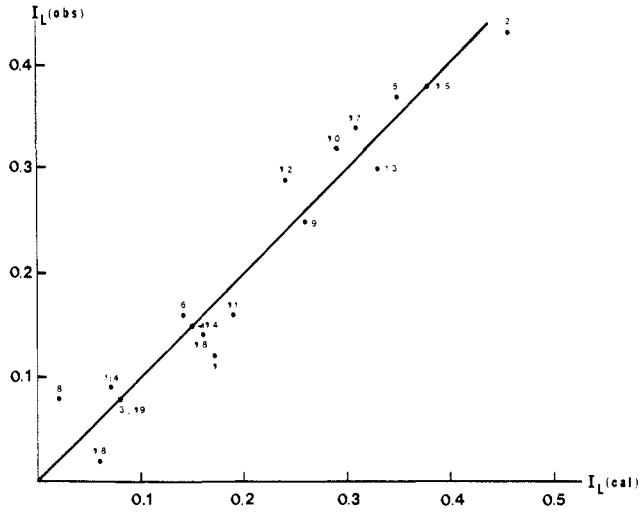

Figure 4. Plot of observed vs calculated ligand intensity I_L.

interactions of two fundamental modes.[24,25] The excellent agreement between theory and experiment is illustrated in Figure 4. The greater scatter at low values of I_L is the result of greater experimental uncertainty in determining the intensities of weak bands.

While the existence of such complications underscore the need for high-quality spectra and cautious interpretation, the present study demonstrates the potential utility of such vibrational interactions. Thus, utilization of multiple isotopomers and careful analysis of resulting spectra can provide accurate estimates for the frequencies of some coordinated histidylimidazole internal modes; information which is otherwise not directly available.[30]

Finally, it is interesting to consider other possible coupling interactions and their potential utility. Thus, we are now making efforts to identify such interactions in dioxygen, carbon monoxide, nitric oxide, and cyanide derivatives of heme proteins and model systems. Such studies are generally focussed on the low frequency region where modes such as ν(Fe–CN), ν(Fe–NO), ν(Fe–CO), ν(Fe–O_2), δ(FeOO), δ(FeCO), δ(FeCN), ν(Co–O_2), and δ(CoOO) may interact with lower frequency histidylimidazole modes. In this way, additional histidylimidazole modes, including ν(Fe–N_{his}), may be observed.

Acknowledgment. We express our sincere thanks to Professor Dennis Strommen of Carthage College for help with the BASIC program and Professor Jeanne McHale for providing a copy of her manuscript prior to publication. L.M.P. acknowledges Grant No. RP-11-13 provided by the Polish Ministry of Education. This work was supported by the National Institutes of Health (Grant No. DK35153 to J.R.K.).

Registry No. O_2, 7782-44-7; Λ-[Co(en)$_2$(*S*-Ala)]$^{2+}$, 28459-63-4; Δ-[Co(en)$_2$(*S*-Ala)]$^{2+}$, 28536-95-0; Λ-[Co(en)$_2$(*S*-Phe)]I_2, 123881-50-5; Δ-[Co(en)$_2$(*S*-Phe)]I_2, 123881-51-6; Λ-[Co(en)$_2$(*S*-Phe)]$(ClO_4)_2$, 123881-52-7; Δ-[Co(en)$_2$(*S*-Phe)]$(ClO_4)_2$, 39000-16-3; Λ-[Co(en)$_2$(*S*-Val)]I_2, 123881-53-8; Δ-[Co(en)$_2$(*S*-Val)]I_2, 123881-54-9; Λ-[Co(en)$_2$(*S*-Val)]Br_2, 123881-55-0; Δ-[Co(en)$_2$(*S*-Val)]Br_2, 123881-56-1; Λ-[Co(en)$_2$(*S*-Glu)]ClO_4, 16040-63-4; Δ-[Co(en)$_2$(*S*-Glu)]ClO_4, 33293-37-7; Λ-[Co(en)$_2$(*S*-Asp)]ClO_4, 33864-49-2; Δ-[Co(en)$_2$(*S*-Asp)]ClO_4, 33864-50-5; Δ,Λ-[Co(en)$_2$(*S*,*R*-AspH)]Cl_2, 123932-07-0; Δ,Λ-[Co(en)$_2$(*R*,*S*-Val)]Cl_2, 123881-57-2; Λ-[Co(en)$_2$(Gly)]$^{2+}$, 19657-80-8; Δ-[Co(en)$_2$(Gly)]$^{2+}$, 19657-79-5; H_2, 1333-74-0.

(30) Caswell, D. S.; Spiro, T. G. *J. Am. Chem. Soc.* **1986**, *108*, 6470.

Phosphate Ester and Phosphinate Binding to the (μ-Oxo)diiron(III) Core: Synthesis and Characterization of $[Fe_2O\{O_2P(OC_6H_5)_2\}_2(HBpz_3)_2]$ and $[Fe_2O\{O_2P(C_6H_5)_2\}_2(HBpz_3)_2]$

Petra N. Turowski, William H. Armstrong, Mary E. Roth, and Stephen J. Lippard*

Contribution from the Department of Chemistry, Massachusetts Institute of Technology, Cambridge, Massachusetts 02139. *Received June 7, 1989*

Abstract: To model the interaction of phosphate ligands with oxo-bridged diiron proteins, (μ-oxo)bis(μ-diphenyl phosphato)bis(hydrotris(1-pyrazolyl)borato)diiron(III) (**1**) and (μ-oxo)bis(μ-diphenylphosphinato)bis(hydrotris(1-pyrazolyl)borato)diiron(III) (**2**) were prepared. X-ray crystallographic studies reveal that the diiron(III) core is expanded in both compounds relative to dicarboxylate-bridged proteins and model compounds. Fe–O–Fe bond angles of 134.7 (2) and 130.6 (3)°, and Fe···Fe distances of 3.335 (1) and 3.292 (2) Å were observed for **1** and **2**, respectively, and the symmetric Fe–O–Fe stretching vibrations at 478 and 485 cm^{-1} have lower energies than those of other triply-bridged diiron(III) compounds. The Fe–O_{oxo} bond distances in **1** and **2**, 1.808 (3) and 1.812 (3) Å, are longer than observed in analogous dicarboxylate bridged compounds, and, consequently, the antiferromagnetic spin exchange coupling constants, −97.5 (1) and −93 (1) cm^{-1}, are smaller in magnitude than usually found in such oxo-bridged diiron(III) compounds. Interactions with the paramagnetic metal centers shift the ^1H NMR signals by up to 6.5 ppm downfield from free ligand values. NMR assignments were facilitated by determination of T_1 relaxation times. As for purple acid phosphatases, no signals were observed in the ^{31}P NMR spectra of either model compound. Mössbauer and electronic spectral parameters resemble those of dicarboxylate-bridged (μ-oxo)diiron(III) model compounds. The phosphate ester and phosphinate bridged model complexes do not exhibit the unusual spectroscopic features of purple acid phosphatases, suggesting that these proteins are unlikely to have a (μ-oxo)(μ-phosphato)diiron(III) center.

Interactions of phosphate[1] ligands with oxo-bridged diiron units are potentially important in proteins such as purple acid phosphatases from bovine spleen[2] and porcine allantoic fluid,[3] ribonucleotide reductase from *E. coli*,[4] the invertebrate respiratory

0002-7863/90/1512-681$02.50/0 © 1990 American Chemical Society

protein hemerythrin,[5] and the mammalian iron storage protein ferritin.[6] Ribonucleotide reductases catalyze the reduction of nucleoside diphosphate substrates in the first committed step of DNA biosynthesis.[4] It is possible that the substrate binds at the oxo-bridged diiron core of the enzyme.[7] Iron phosphate interactions may be important in hemerythrin as well, since it has recently been shown that aminoethyl phosphate or aminoethyl phosphonate species occur in sipunculan erythrocytes at concentrations approaching 0.1 M.[5a] These phosphate compounds bind weakly to hemerythrin, inducing changes in the properties of the (μ-oxo)diiron center.[5a] Furthermore, the iron oxo/hydroxo core in ferritin is well-known to contain inorganic phosphate.[6]

Purple acid phosphatases catalyze the hydrolysis of phosphate esters under acidic conditions.[8] One proposal for the diiron(III) site of oxidized beef spleen purple acid phosphatase (BPAP) includes an inorganic phosphate ligand bound to one of the iron atoms.[2a] Studies of inorganic phosphate binding to purple acid phosphatase isolated from the uterine fluid of pregnant or pseudopregnant sows (uteroferrin, Uf) led to the postulate that two iron atoms are bridged by inorganic phosphate in the oxidized (Fe^{III},Fe^{III}) form of the protein.[8] The two iron atoms in oxidized purple acid phosphatases are strongly antiferromagnetically coupled and exhibit large quadrupole splittings values and short Fe···Fe distances, all of which suggest the presence of an oxo bridge.[8] A short Fe–O_{oxo} bond is not consistent with the EXAFS data, however, nor has the expected strong symmetric Fe–O–Fe stretching vibration been unambiguously identified in Raman studies of the proteins,[2a] so that the presence of an oxo bridge remains questionable.[8]

To augment our understanding of the diiron cores of these proteins, we have prepared two oxo-bridged diiron(III) complexes containing phosphate ligands, $[Fe_2O\{O_2P(OC_6H_5)_2\}_2(HBpz_3)_2]$ (**1**) and $[Fe_2O\{O_2P(C_6H_5)_2\}_2(HBpz_3)_2]$ (**2**), where $(HBpz_3)^-$ is hydrotris(1-pyrazolyl)borate. We describe the characterization of these complexes by crystallographic and electrochemical methods, by magnetic susceptometry, and by Mössbauer, NMR, resonance Raman, and UV/vis/NIR spectroscopies. Preliminary results for **1** were communicated previously,[7] and EXAFS results for this complex were published separately.[9] These compounds were derived from $[Fe_2O(O_2CCH_3)_2(HBpz_3)_2]$ (**3**)[10] in an ongoing program to model dinuclear iron oxo centers in biology.[7,10,11] Prior to the characterization of these phosphate-bridged compounds, only polymeric iron(III) phosphate minerals had been crystallographically characterized,[12] so that the complexes presented here add considerably to our understanding of iron(III) phosphate interactions. The properties of **1** and **2** are compared to those of uteroferrin and beef spleen purple acid phosphatase.

Experimental Section

Materials and Methods. $[Fe_2O(O_2CCH_3)_2(HBpz_3)_2]$ (**3**) was prepared as previously described.[10] For electrochemistry experiments, solvents and electrolytes were of electrochemistry grade or purified by distillation or recrystallization, respectively, prior to their use. All other reagents were obtained from commercial sources and used as supplied. ^{18}O-enriched (99%) water was supplied by Stohler Isotope Laboratories, Waltham, MA. Mössbauer spectra of samples in a BN matrix were recorded at the Francis Bitter National Magnet Laboratory as previously described.[11a] ^1H NMR spectra and T_1 measurements were obtained on a Varian XL 300 instrument by using tetramethylsilane as an internal reference standard, and ^{31}P spectra were obtained on Varian XL 300, XL 400, and VXL 500 spectrometers by using 80% H_3PO_4 as an external reference standard. All NMR experiments were carried out at room temperature in CD_2Cl_2. Fast atom bombardment (FAB) mass spectra in glycerol or *p*-(nitrophenoxy)octane matrices were recorded on a Finnigan MAT System 8200 instrument equipped with an FAB gun using xenon atoms as the source. Ultraviolet and visible spectra were obtained on a Varian Lambda 7 instrument, and near-infrared spectra were recorded with a Perkin Elmer Model 300 spectrophotometer. Fourier transform infrared spectroscopy on KBr pellets was performed on IBM IR/32 and Mattson Cygnus 400 instruments.

Several lines from an argon ion laser (Coherent Radiation Model 52, Spectra Physics Model 164, and Innovia Model 70) were used to obtain resonance Raman spectra of **1** and **2** in CH_2Cl_2 as described previously.[13] For the resonance Raman excitation profile of **1**, saturated (~0.2 M) solutions were sealed in capillaries and held stationary in the beam with a 90° geometry, where the beam was passed through the sample close to the edge of the capillary to prevent absorption. The power incident at the sample was 10–50 mW, with slits set at 300/400/300 μm. The compound was stable during excitation at all wavelengths, as determined by visible spectroscopy. The excitation profile of a given peak was determined by comparing its height with that of the C–Cl stretching vibration of CH_2Cl_2 at 704 cm^{-1} as a function of excitation wavelength. No correction for sample absorption was made.

Cyclic voltammetry experiments were performed with a Princeton Applied Research Model 173 potentiostat and Model 175 universal programmer or on a Pine Instruments RDE4 apparatus and recorded on a Houston Instruments Model 2000 or Kipp & Zonen BD 91 X-Y recorder. The supporting electrolyte was 0.1 M tetra-*n*-butylammonium perchlorate in methylene chloride or 0.1 M lithium perchlorate in acetonitrile. A platinum disc working electrode, a platinum wire auxilliary electrode, and a silver/silver chloride reference electrode fitted with a vycor plug at the solution junction were employed.

Preparation of Compounds. **(μ-Oxo)bis(μ-diphenyl phosphato)bis(hydrotris(1-pyrazolyl)borato)diiron(III), $[Fe_2O\{O_2P(OC_6H_5)_2\}_2(HBpz_3)_2]$ (1).** A solution of 0.742 g (2.97 mmol) of $HO_2P(OC_6H_5)_2$ in 50 mL of CH_2Cl_2 was added dropwise over 5 min to a solution of 1.002 g (1.491 mmol) of $[Fe_2O(O_2CCH_3)_2(HBpz_3)_2]$ (**3**) in 500 mL of CH_2Cl_2. A rapid color change from brown-green to emerald green indicated that the reaction proceeded readily. After the reaction mixture was stirred for 1 h, the solvent was removed with a rotary evaporator. The resulting dark green oil was dissolved in 30 mL of CCl_4 and allowed to stand for 3 days at ambient temperature. The microcrystalline green solid which formed was filtered, washed with 10 mL of CCl_4 and 2 × 10 mL portions of hexanes, powdered, and dried under vacuum. This procedure afforded

(1) Phosphate, as used here, includes phosphates, phosphonates, phosphinates, and their esters.

(2) (a) Averill, B. A.; Davis, J. C.; Burman, S.; Zirino, T.; Sanders-Loehr, J.; Loehr, T. M.; Sage, J. T.; DeBrunner, P. G. *J. Am. Chem. Soc.* **1987**, *109*, 3760–3767. (b) Kauzlarich, S. M.; Teo, B. K.; Zirino, T.; Burman, S.; Davis, J. C.; Averill, B. A. *Inorg. Chem.* **1986**, *25*, 2781–2787. (c) Doi, K.; Antanaitis, B. C.; Aisen, P. *Struct. Bonding* **1988**, *70*, 1–26. (d) Davis, J. C.; Lin, S. S.; Averill, B. A. *Biochemistry* **1981**, *20*, 4062–4067.

(3) (a) Pyrz, J. W.; Sage, J. T.; Debrunner, P. G.; Que, L., Jr. *J. Biol. Chem.* **1986**, *261*, 11015–11020. (b) Sinn, E.; O'Connor, C. J.; de Jersey, J.; Zerner, B. *Inorg. Chim. Acta* **1983**, *78*, L13–L15. (c) Debrunner, P. G.; Hendrich, M. P.; de Jersey, J.; Keogh, D. T.; Zerner, B. *Biochim. Biophys. Acta* **1983**, *745*, 103–106. (d) Antanaitis, B. C.; Aisen, P.; Lilienthal, H. R. *J. Biol. Chem.* **1983**, *258*, 3166–3172.

(4) (a) Sjöberg, B.-M.; Gräslund, A. *Adv. Inorg. Biochem.* **1983**, *5*, 87–110. (b) Scarrow, R. C.; Maroney, M. J.; Palmer, S. M.; Que, L., Jr.; Roe, A. L.; Salowe, S. P.; Stubbe, J. *J. Am. Chem. Soc.* **1987**, *109*, 7857–7864. (c) Backes, G.; Sahlin, M.; Sjöberg, B.-M.; Loehr, T. M.; Sanders-Loehr, J. *Biochemistry* **1989**, *28*, 1923–9.

(5) (a) Robitaille, P.-M.; Kurtz, D. M. *Biochemistry* **1988**, *27*, 4458–4465. (b) Stenkamp, R. E.; Sieker, L. C.; Jensen, L. H. *J. Am. Chem. Soc.* **1984**, *106*, 618–622. (c) Shiemke, A. K.; Loehr, T. M.; Sanders-Loehr, J. *J. Am. Chem. Soc.* **1984**, *106*, 4951–4956.

(6) Theil, E. C. *Adv. Inorg. Biochem.* **1983**, *5*, 1–38.

(7) Armstrong, W. H.; Lippard, S. J. *J. Am. Chem. Soc.* **1985**, *107*, 3730–3731.

(8) Que, L., Jr.; Scarrow, R. C. In *Metal Clusters in Proteins*; Que, L., Jr., Ed.; ACS Symposium Series No. 372; American Chemical Society: Washington, DC, 1988; pp 152–178.

(9) Hedman, B.; Co, M. S.; Armstrong, W. H.; Hodgson, K. O.; Lippard, S. J. *Inorg. Chem.* **1986**, *25*, 3708–3711.

(10) (a) Armstrong, W. H.; Spool, A.; Papaefthymiou, G. C.; Frankel, R. B.; Lippard, S. J. *J. Am. Chem. Soc.* **1984**, *106*, 3653–3667. (b) Armstrong, W. H.; Lippard, S. J. *J. Am. Chem. Soc.* **1983**, *105*, 4837–4838.

(11) (a) Hartman, J. R.; Rardin, R. L.; Chaudhuri, P.; Pohl, K.; Wieghardt, K.; Nuber, B.; Weiss, J.; Papaefthymiou, G. C.; Frankel, R. B.; Lippard, S. J. *J. Am. Chem. Soc.* **1987**, *109*, 7387–7396. (b) Spool, A.; Williams, I. D.; Lippard, S. J. *Inorg. Chem.* **1985**, *24*, 2156–2162. (c) Armstrong, W. H.; Lippard, S. J. *J. Am. Chem. Soc.* **1984**, *106*, 4632–4633. (d) Feng, X.; Bott, S. G.; Lippard, S. J. *J. Am. Chem. Soc.* **1989**, *111*, 8046–8047. (e) Lippard, S. J. *Angew. Chem., Int. Ed. Engl.* **1988**, *27*, 344–364. (f) Tolman, W. B.; Bino, A.; Lippard, S. J. *J. Am. Chem. Soc.* **1989**, *111*, 8522–8523. (g) Beer, R. H.; Tolman, W. B.; Bott, S. G.; Lippard, S. J. *Inorg. Chem.* In press.

(12) (a) Bosman, W. P.; Beurskens, P. T.; Smits, J. M. M.; Behm, H.; Mintjens, J.; Meisel, W.; Fuggle, J. C. *Acta Crystallogr.* **1986**, *C42*, 525–528. (b) Mansour, A. N.; Thompson, C.; Theil, E. C.; Chasteen, N. D.; Sayers, D. E. *J. Biol. Chem.* **1985**, *260*, 7975–7979. (c) Meisel, W.; Guttmenn, H. T.; Gutlich, P. *Corros. Sci.* **1983**, *23*, 1373–1379.

(13) Armstrong, W. H.; Roth, M. E.; Lippard, S. J. *J. Am. Chem. Soc.* **1987**, *109*, 6318–6326.

1.394 g (78%) of the CCl_4 solvate of **1** (by elemental analysis). Purification of the complex was achieved by recrystallization from $CHCl_3$ with hexanes carefully layered on top to yield dark green block-shaped crystals which analyzed well for **1**·$CHCl_3$. Crystals of **1**·$CHCl_3$ obtained by this method were suitable for X-ray diffraction studies. ^1H NMR (250 MHz, CD_2Cl_2) δ 13.8 ppm (br), ~12.7 sh, ~10.9 sh, 7.9 sh, 7.37, 7.27, 7.15, ~2.5 (br); IR (KBr) 3075 cm^{-1}, 3054, 2482 (B–H), 1592, 1491, 1403, 1391, 1310, 1214, 1203, 1164, 1110, 1083, 1049, 1028, 1008, 982, 942, 935, 930, 906, 887, 816, 763, 729, 718, 691, 662, 658, 622, 537, 522; Raman (457.9 nm, CH_2Cl_2) 1406 cm^{-1}, 1390, 1311, 1220, 1193, 1108, 1006, 950, 929, 478, 370, 282, 214; FAB-MS (*m/e*) 1053 (M + H), 1036 (M – O), 965 (M – pz), 918 (M – 2pz), 804 (M – $O_2P(OC_6H_5)_2$), 590 (M – $O_2P(OC_6H_5)_2$ – $HBpz_3$), 520 (M – Fe – O – $O_2P(OC_6H_5)_2$ – $HBpz_3$). Anal. Calcd for $C_{43}H_{41}B_2Cl_3Fe_2N_{12}O_9P_2$: C, 44.09; H, 3.53; Cl, 9.08; Fe, 9.53; N, 14.35; P, 5.29. Found: C, 44.11; H, 3.49; Cl, 9.01; Fe, 9.50; N, 14.39; P, 5.23. $[Fe_2{}^{18}O\{O_2P(OC_6H_5)_2\}_2(HBpz_3)_2]$ was prepared by analogy to the synthesis of $[Fe_2{}^{18}O(O_2CCH_3)_2(HBpz_3)_2]$, namely by oxo ligand exchange with ^{18}O-enriched water.[10] Product **1** could also be obtained by a method similar to that reported for $[Fe_2O(O_2CC_6H_5)_2(HBpz_3)_2]$,[10] employing $KO_2P(OC_6H_5)_2$ instead of $KO_2CC_6H_5$. This procedure afforded lower yields of **1** (10%) than the method described above.

(μ-Oxo)bis(μ-diphenylphosphinato)bis(hydrotris(1-pyrazolyl)borato)diiron(III), $[Fe_2O\{O_2P(C_6H_5)_2\}_2(HBpz_3)_2]$ (2). This compound was prepared in a similar fashion to **1**, by adding 0.521 g (2.39 mmol) of diphenylphosphinic acid to 0.998 g (1.193 mmol) of **3**·4CH_3CN in 500 mL of CH_2Cl_2. The product, a dark green oil, was dissolved in 30 mL of CCl_4, and the mixture was filtered to remove a red precipitate containing $[Fe(HBpz_3)_2]^+$. The filtrate was allowed to stand for 3 days at ambient temperature. The dark green crystals that formed were separated by filtration and washed with 10 mL of CCl_4 to yield 0.642 g (42%) of **2**·CH_2Cl_2·CCl_4. This formulation of the material was reproducibly obtained, as determined by X-ray crystallography and elemental analysis. Crystals were also obtained by slow evaporation from acetonitrile (**2**·3CH_3CN, by X-ray crystallography) or from chloroform. ^1H NMR (300 MHz, CD_2Cl_2) δ 14.1 ppm (br), 13.8 (br), 11.2 (br), 10.8 (br), 8.5 sh, 8.12, 7.95, 7.58, 7.34, 7.12, 2.9 (br); IR (KBr) 3075 cm^{-1}, 3054, 2475 (B–H), 1501, 1439, 1422, 1418, 1403, 1390, 1257, 1213, 1202, 1145, 1136, 1131, 1114, 1094, 1066, 1049, 1037, 1023, 1014, 996, 980, 791, 756, 728, 716, 702, 693, 662, 622, 557, 549, 537, 471; Raman (514.5 nm, CH_2Cl_2) 1594 cm^{-1}, 1406, 1390, 1310, 1221, 1188, 1092, 1022, 998, 927, 485, 308, 246, 209; FAB-MS (*m/e*) 989 (M + H), 971 (M – OH), 920 (M – pz – H), 771 (M – $O_2P(C_6H_5)_2$), 503 (M – Fe – $O_2P(C_6H_5)_2$ – $HBpz_3$ + H), 486 (M – Fe – O – $O_2P(C_6H_5)_2$ – $HBpz_3$). Anal. Calcd for $C_{44}H_{42}B_2Cl_6Fe_2N_{12}O_5P_2$: C, 43.08; H, 3.45; Cl, 17.34; Fe, 9.10; N, 13.70; P, 5.05. Found: C, 42.87; H, 3.51; Cl, 17.40; Fe, 9.19; N, 13.81; P, 4.93.

X-ray Crystallography. A large dark green (almost black) crystal of **1**·$CHCl_3$ was flame-sealed in a glass capillary to prevent solvent loss from the lattice. It belonged to the monoclinic crystal system, as did the dark green block-shaped crystal of **2**·CH_2Cl_2·CCl_4 that was selected and mounted with epoxy resin on a thin glass fiber. Relevant crystallographic information is presented in Table I. Unit cell parameters and intensity data were obtained by using the general procedures previously described.[14] Corrections were applied for Lorentz and polarization effects, but it was unnecessary to account for crystal decay. An empirical absorption correction was applied to the **2**·CH_2Cl_2·CCl_4 data but not to that of **1**·$CHCl_3$. The structures of both compounds were solved by using the direct methods program MULTAN and standard difference Fourier methods in the TEXSAN package.[15] The positions of all non-hydrogen atoms were refined with anisotropic thermal parameters, and the H atom positions were placed at calculated positions for the final refinement cycles. The disorder observed for atoms Cl2 and Cl3 of the CCl_4 molecule of **2**·CH_2Cl_2·CCl_4 was modeled by anisotropic refinement of two positions at half occupancy each. Large anisotropic thermal ellipsoids on C13–C15 and C22–C24 of the two phenyl rings suggested disorder that was not modeled. For both **1**·$CHCl_3$ and **2**·CH_2Cl_2·CCl_4, the largest remaining electron density maxima (1.20 and 0.44 $eÅ^{-3}$, respectively) and minima (–0.62 and –0.52 $eÅ^{-3}$, respectively) on Fourier difference maps appeared near the solvent molecules and may correspond to unresolved partial disorder. Final refinement parameters are given in Table I, and selected bond distances and angles are provided in Table II. Listings of observed and calculated structure factors for **1**·$CHCl_3$ and **2**·CH_2Cl_2·CCl_4 may be found in Supplementary Material Tables S1 and S2. Final thermal parameters for all non-hydrogen atoms are supplied in Tables S3 and S4, positional parameters for all atoms are given in Tables S5 and S6, and full lists of bond distances and angles may be found in Tables S7 and S8.

Table I. Crystallographic Information for $[Fe_2O\{O_2P(OC_6H_5)_2\}_2(HBpz_3)_2]$·$CHCl_3$, **1**, and $[Fe_2O\{O_2P(C_6H_5)_2\}_2(HBpz_3)_2]$·$CH_2Cl_2$·$CCl_4$, **2**[a]

	1	**2**
formula	$C_{43}H_{41}B_2Cl_3Fe_2N_{12}O_9P_2$	$C_{44}H_{42}B_2Cl_6Fe_2N_{12}O_5P_2$
formula wt, g mol^{-1}	1171.5	1226.9
space group	$P2_1/n$	$C2/c$
a, Å	11.940 (2)	18.373 (1)
b, Å	20.105 (4)	15.518 (1)
c, Å	22.155 (3)	19.986 (1)
β, deg	96.56 (1)	105.315 (4)
V, $Å^3$	5284 (3)	5496 (1)
Z	4	4
D_{calcd}, g cm^{-1}	1.473	1.483
D_{obsd},[b] g cm^{-1}	1.48 (1)	1.48 (1)
radiation	Mo Kα (0.71073 Å)	Mo Kα (0.71073 Å)
abs coeff, cm^{-1}	8.2	9.3
data collected	$3° \le 2\theta \le 46°$, $+h,+k,\pm l$	$3° \le 2\theta \le 32°$, $\pm h,+k,\pm l$; $3° \le 2\theta \le 50°$, $+h,+k,\pm l$
total no. of data collected	8010	6719
total no. of unique data	7591	5017
no. of unique data with $I > 3\sigma(I)$	4674	2631
no. of variable param	658	350
R_1[c]	0.044	0.058
R_2[c]	0.063	0.070

[a] All measurements were made at room temperature. [b] By suspension in a mixture of CCl_4 and toluene. [c] $R_1 = \sum||F_o| - |F_c||/\sum|F_o|$; $R_2 = [\sum w||F_o| - |F_c||^2/\sum w|F_o|^2]^{1/2}$, where $w = 1/\sigma^2(F_o)$.

Magnetic Susceptibility Measurements. The solution magnetic susceptibilities of **1** and **2**·CH_2Cl_2·CCl_4 were measured in CD_2Cl_2 by the Evans NMR technique,[16] by using diamagnetic corrections of -581.4×10^{-6} cgs mol^{-1} and -633.1×10^{-6} cgs mol^{-1}, respectively, calculated from Pascal's constants.[17] Solid-state measurements of 21.31 mg of powdered **1** in an Al–Si sample container and 113.0 mg of powdered **2**·CH_2Cl_2·CCl_4 in a polyethylene sample container were carried out at the Francis Bitter National Magnet Laboratory with an S.H.E. Model 905 SQUID susceptometer at 20 and 10 kG, respectively. A total of 45–48 data points was taken over the range 5–300 K. The moment of the sample holders was measured at the same temperature points and subtracted from the observed moment with sample present. Theoretical expressions used to fit the data were described previously.[11a,18] For **1**, the antiferromagnetic coupling constant, *J*, and the paramagnetic impurity term, *p*, were allowed to vary during the refinement, and, for **2**, a Weiss term (θ) was included in the expression to obtain an acceptable fit to the data.

Results and Discussion

Syntheses. To avoid formation of polymeric iron phosphate materials and of the $[Fe(HBpz_3)_2]^+$ cation, we used starting materials containing the $\{Fe_2O\}^{4+}$ core. The oxo bridge in **3** is easily exchanged with ^{18}O-labeled water to form $[Fe_2{}^{18}O(O_2CCH_3)_2(HBpz_3)_2]$.[10] Exchange with CD_3OOD produces $[Fe_2O(O_2CCD_3)_2(HBpz_3)_2]$.[7] Phosphate-bridged complexes could be readily prepared in a similar fashion, as described in eq 1, where

$$[Fe_2O(O_2CCH_3)_2(HBpz_3)_2] + 2R_2PO_2H \xrightarrow{CH_2Cl_2} [Fe_2O(O_2PR_2)_2(HBpz_3)_2] + 2CH_3CO_2H \quad (1)$$

R = OC_6H_5 or C_6H_5. $[Fe_2O\{O_2P(OC_6H_5)_2\}_2(HBpz_3)_2]$ (**1**) and $[Fe_2O\{O_2P(C_6H_5)_2\}_2(HBpz_3)_2]$ (**2**) were assembled in this manner in good yields (42–78% after crystallization). The yield of **2** is lower since the compound slowly decomposes in solution to form

(14) Silverman, L. D.; Dewan, J. C.; Giandomenico, C. M.; Lippard, S. J. *Inorg. Chem.* **1980**, *19*, 3379–3383.

(15) TEXRAY Structure Analysis Package, Molecular Structure Corporation, College Station, TX, 1985.

(16) (a) Evans, D. F. *J. Chem. Soc.* **1958**, 2003–2005. (b) Live, D. H.; Chan, S. I. *Anal. Chem.* **1970**, *42*, 791–792.

(17) (a) Carlin, R. L. In *Magnetochemistry*; Springer-Verlag: New York, 1986; pp 3–33. (b) O'Connor, C. J. *Prog. Inorg. Chem.* **1982**, *29*, 203–283.

Table II. Selected Interatomic Distances (Å) and Angles (deg) for $[Fe_2O\{O_2P(OC_6H_5)_2\}_2(HBpz_3)_2]\cdot CHCl_3$, **1**, and $[Fe_2O\{O_2P(C_6H_5)_2\}_2(HBpz_3)_2]\cdot CH_2Cl_2\cdot CCl_4$, **2**[a]

1		2	
Fe1···Fe$_2$	3.335 (1)	Fe···Fe″	3.292 (2)
Fe1–O, Fe2–O	1.807 (3), 1.808 (3)	Fe–O	1.812 (3)
Fe1–O11, Fe1–O12	2.059 (4), 2.038 (4)	Fe–O1	2.013 (4)
Fe2–O21, Fe2–O22	2.039 (4), 2.038 (4)	Fe–O2	2.013 (4)
Fe1–N11, Fe1–N17	2.136 (5), 2.113 (4)	Fe–N1	2.174 (6)
Fe2–N21, Fe2–N27	2.124 (5), 2.142 (4)	Fe–N7	2.177 (5)
Fe1–N14, Fe2–N24	2.208 (4), 2.219 (5)	Fe–N4	2.171 (5)
Fe1···P1, Fe1···P2	3.216 (2), 3.209 (2)	Fe···P	3.208 (2)
Fe2···P1, Fe2··P2	3.215 (2), 3.202 (2)	Fe···P″	3.223 (2)
O–Fe1–O11, O–Fe1–O12	94.7 (1), 95.2 (1)	O–Fe–O1	95.8 (2)
O–Fe2–O21, O–Fe2–O22	95.6 (1), 94.5 (1)	O–Fe–O2	95.8 (2)
O–Fe1–N11, O–Fe1–N17	98.2 (2), 97.8 (2)	O–Fe–N1	97.4 (2)
O–Fe2–N21, O–Fe2–N27	98.0 (2), 98.7 (2)	O–Fe–N4	95.0 (2)
O–Fe1–N14, O–Fe2–N24	179.8 (2), 178.8 (2)	O–Fe–N7	177.0 (2)
O11–Fe1–O12, O21–Fe2–O22	91.7 (2), 89.4 (2)	O1–Fe–O2	92.5 (2)
O11–Fe1–N11, O11–Fe1–N14	88.9 (2), 85.6 (1)	O1–Fe–N1	90.7 (2)
O12–Fe1–N14, O12–Fe2–N17	84.8 (2), 90.9 (2)	O1–Fe–N7	86.2 (2)
O21–Fe2–N21, O21–Fe2–N24	91.5 (2), 84.8 (2)	O2–Fe–N4	91.5 (2)
O22–Fe2–N24, O22–Fe2–N27	84.3 (2), 91.2 (2)	O2–Fe–N7	84.4 (2)
O11–Fe1–N17, O12–Fe1–N11	166.9 (1), 166.5 (2)	O1–Fe–N4	167.0 (2)
O21–Fe2–N27, O22–Fe2–N21	165.6 (2), 167.3 (2)	O2–Fe–N1	165.9 (2)
N11–Fe1–N14, N21–Fe2–N24	81.9 (2), 83.1 (2)	N1–Fe–N4	82.5 (2)
N11–Fe1–N17, N21–Fe2–N27	85.6 (2), 84.8 (1)	N1–Fe–N7	82.2 (2)
N14–Fe1–N17, N24–Fe2–N27	81.9 (2), 81.0 (2)	N4–Fe–N7	82.0 (2)
P1–O11, P1–O21	1.484 (4), 1.486 (4)	P–O1	1.511 (4)
P2–O12, P2–O22	1.483 (4), 1.483 (4)	P–O2	1.504 (5)
P1–O31, P1–O32	1.581 (4), 1.578 (4)	P–C10	1.790 (7)
P2–O41, P2–O42	1.596 (4), 1.573 (4)	P–C20	1.791 (7)
O11···O21, O12···O22	2.569 (2), 2.574 (5)	O1···O2″	2.564 (6)
O11–P1–O21, O12–P2–O22	119.8 (2), 120.4 (2)	O1–P–O2″	116.5 (2)
C10–C11	1.671 (8)	C30–C11	1.678 (9)
C10–C12	1.81 (1)	C40–C12	1.706 (8)
C10–C13	1.663 (9)	C40–C12′	1.65 (9)
		C40–C13	1.55 (1)
		C40–C13′	1.969 (9)

	min	max	mean	min	max	mean
O–C	1.402 (7)	1.428 (7)	1.410			
C–C$_{phenyl}$	1.29 (1)	1.41 (1)	1.37	1.29 (1)	1.38 (1)	1.37
B–N	1.518 (8)	1.552 (9)	1.538	1.52 (1)	1.55 (1)	1.54
N–N	1.345 (6)	1.370 (6)	1.359	1.357 (7)	1.367 (7)	1.361
C–N	1.315 (7)	1.341 (7)	1.331	1.305 (8)	1.357 (9)	1.329
C–C$_{pyrazole}$	1.34 (1)	1.395 (8)	1.371	1.33 (1)	1.39 (1)	1.37

[a] See Figure 1 for labeling schemes. Estimated standard deviations, in parentheses, occur in the last significant figure. The second of two disordered atom positions is indicated by (′), and (″) identifies an atom related by the C_2 operator. No corrections for thermal motion were made.

a pale yellow precipitate. The substitution reaction (eq 1) proceeds readily for phosphate monoacids of general formula $(RO)_2PO_2H$ or R_2PO_2H but not for di- or triprotic acids such as $ROPO_3H_2$, RPO_3H_2, H_3PO_4, or their salts. Addition of such species to solutions containing **3** causes an immediate bleaching of the green color and generation of a pale yellow precipitate that appears to be a polymeric iron phosphate material, based on its lack of solubility and infrared spectrum. An alternate route to **1** and **2** involves the use of $(Et_4N)_2[Fe_2OCl_6]$,[19] already known to be a valuable starting material for preparing triply-bridged diiron(III) oxo complexes.[10] This route gives lower yields, however, producing larger amounts of the red $[Fe(HBpz_3)_2]^+$ cation, a major side product in both types of reactions.

Crystallographic Results. The structures of **1**·$CHCl_3$ and **2**·$CH_2Cl_2\cdot CCl_4$ are shown in Figure 1, and Table II contains selected geometric information. Compound **2** has crystallographically imposed C_2 symmetry. The structures reveal that the oxo-bridged diiron(III) core is retained upon exchange of carboxylate with diphenyl phosphate or diphenylphosphinate ligands. The (μ-oxo)diiron(III) core is now bridged by two bidentate phosphate ligands, and the resulting $\{Fe_2O(O_2PR_2)_2\}^{2+}$ unit is capped by hydrotris(1-pyrazolyl)borate ligands. The iron atoms in both complexes are distorted octahedral, with the largest deviation from the idealized 90° angles being 9° in **1** and 8° in **2**. Some important structural features of **1** and **2** are compared with those of selected compounds in Table III. The structures of **1** and **2** are quite similar to that of $[Fe_2O(O_2CCH_3)_2(HBpz_3)_2]$ (**3**).[10] The Fe–O_{oxo} distances are slightly longer in **1** and **2** than in **3**, 1.808 (3) and 1.812 (3) Å vs 1.784 (4) Å, respectively. The larger Fe–O–Fe angles, 134.7 (2)° and 130.6 (3)° vs 123.6 (1)°, and resulting greater Fe···Fe separations, 3.335 (1) and 3.292 (2) vs 3.146 (1) Å, in **1** and **2** are presumably due to an increased O···O separation in phosphate[20] or phosphinate[21] compared to carboxylate[10,11b,22]

(18) Karlin, K., Ph.D. Dissertation, Columbia University, 1975.
(19) (a) Armstrong, W. H.; Lippard, S. J.; *Inorg. Chem.* **1985**, *24*, 981–982. (b) Drew, M. G. B.; McKee, V.; Nelson, S. M. *J. Chem. Soc., Dalton Trans.* **1978**, 80–84. (c) Solbrig, R. M.; Duff, L. L.; Shriver, D. F.; Klotz, I. M. *J. Inorg. Biochem.* **1982**, *17*, 69–74.

(20) Taken or, if not supplied, calculated from the following: (a) Day, R. O.; Chandrasekhar, V.; Swamy, K. C. K.; Holmes, J. M.; Burton, S. D.; Holmes, R. R. *Inorg. Chem.* **1988**, *27*, 2887–2893. (b) Narayanan, P.; Ramirez, F.; McCaffrey, T.; Chaw, Y.; Marecek, J. F. *J. Org. Chem.* **1978**, *43*, 24–31. (c) Toney, J. H.; Brock, C. P.; Marks, T. J. *J. Am. Chem. Soc.* **1986**, *108*, 7263–7274.
(21) Taken or, if not supplied, calculated from the following: (a) Swamy, K. C. K.; Schmid, C. G.; Day, R. O.; Holmes, R. R. *J. Am. Chem. Soc.* **1988**, *110*, 7067–7076. (b) Colamarino, P.; Orioli, P. L.; Benzinger, W. D.; Gillman, H. D. *Inorg. Chem.* **1976**, *15*, 800–804. (c) Betz, P.; Bino, A. *Inorg. Chim. Acta* **1988**, *147*, 109–113.

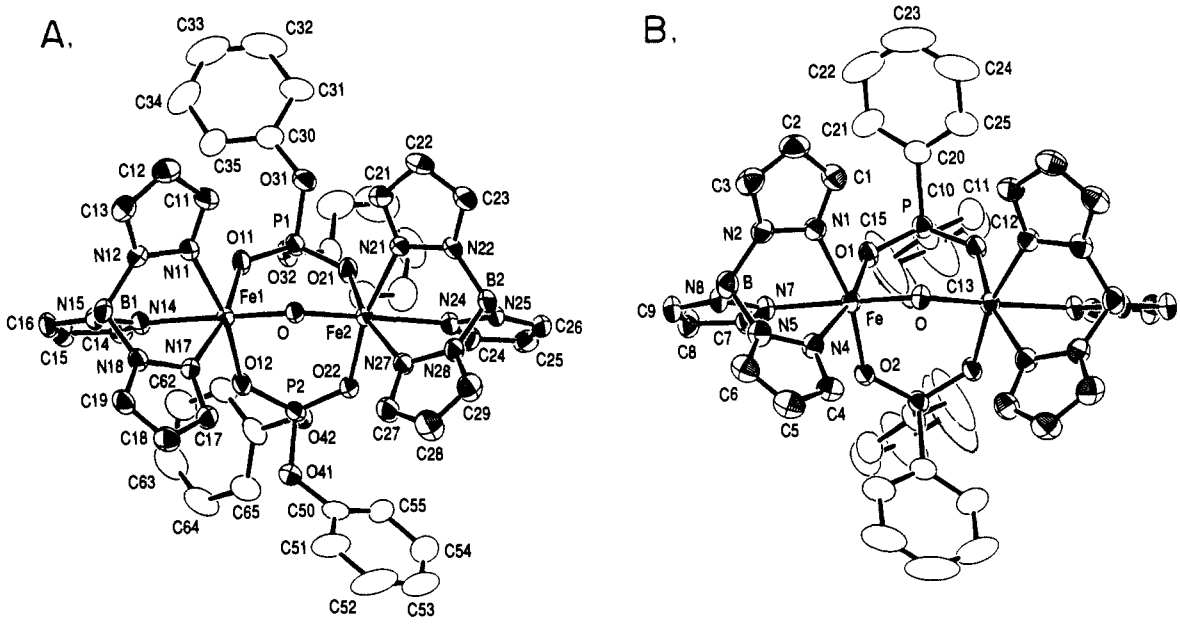

Figure 1. Structures of (A) $[Fe_2O\{O_2P(OC_6H_5)_2\}_2(HBpz_3)_2]\cdot CHCl_3$, **1**·$CHCl_3$, and (B) $[Fe_2O\{O_2P(C_6H_5)_2\}_2(HBpz_3)_2]\cdot CH_2Cl_2\cdot CCl_4$, **2**·$CH_2Cl_2\cdot CCl_4$, showing the 30% probability thermal ellipsoids and the atom labeling schemes. In (A), phenyl rings C40–C45 and C60–C65 are partially obscured, as is phenyl ring C10–C15 in (B).

Table III. Comparison of Structural, Mössbauer, and Magnetic Parameters of Selected Model Compounds and Purple Acid Phosphatases

compd	Fe–O_{short},[a] Å	Fe···Fe, Å	∠Fe–O–Fe,[b] deg	Fe–P_{av}, Å	Fe–OP,C, Å	Fe–N_{av},[c] Å	O···O_{av}, Å	δ, mm/s	ΔE_Q, mm/s	$-J$,[d] cm^{-1}
1	1.808 (3)	3.335 (1)	134.7 (2)	3.211 (2)	2.044 (4)	2.13, 2.21	2.572 (5)	0.53 (3)	1.60 (5)	97.5 (1)
2	1.812 (3)	3.292 (2)	130.6 (3)	3.216 (2)	2.013 (4)	2.174 (6)	2.564 (6)	0.50 (3)	1.57 (3)	95 (1)
3[e]	1.784 (4)	3.149 (1)	123.6 (1)		2.043	2.15, 2.19	2.236 (3)	0.52 (3)	1.60 (5)	121
$Fe_2(OH)$[f]	1.956 (4)	3.439 (1)	123.1 (2)		1.999 (4)	2.102	2.237 (6)	0.47 (3)	0.25	17
Uf_o–P_i[g]	1.96 (2)	3.2	109	3.1–3.2	1.96	2.10		0.52, 0.55	1.02, 1.38	>40
$BPAP_o$–P_i[h]	1.98 (2)	3.01	99	3.1	1.98	2.13		0.51, 0.54	1.03, 1.36	>150

[a] Fe–O_{short} refers to Fe–O_{oxo} and Fe–OH distances. [b] Angles for the proteins are calculated from the relevant distances. [c] Two distances refer to nitrogens cis and trans to the oxo bridge. [d] From temperature dependent magnetic susceptibility studies (model compounds, BPAP) and NMR studies (Uf). [e] Reference 10. [f] $[Fe_2(OH)(O_2CCH_3)_2(HBpz_3)](BF_4)$, ref 11c and 11a (Mössbauer data.) [g] References 8 (EXAFS data), 3a,c (Mössbauer data), and 3b,c (magnetic data). [h] References 2b (EXAFS data) and 2a (Mössbauer and magnetic data).

ligands. The Fe–O–Fe angles for **1** and **2** are unusually large for triply-bridged diiron(III) complexes, being closer to values obtained in a doubly-bridged analogue.[22a] The ligand O···O separation in carboxylate diiron complexes is around 2.23 Å,[10,11b,22] whereas it is 2.572 (5) and 2.564 (6) Å in the diphenyl phosphate and diphenylphosphinate complexes, respectively.[20,21] The expansion of the core in **1** is more pronounced than in **2** because of the slightly longer Fe–OP distances in the former (2.044 vs 2.013 Å). The Fe–OP distance in **1** is comparable to Fe–OC distances in carboxylate-bridged diiron complexes,[10,11,22] whereas the Fe–OP distance in **2** is significantly shorter, reflecting the altered electronic character of the ligand. Diphenylphosphinate and diphenyl phosphate complexes of tin show a similar trend. The Sn–OP bond lengths in the former complex are significantly shorter than those in the latter (2.099 vs 2.155 Å).[20a,21a]

It is notable that there is very little variation among Fe–O or Fe–N bond lengths in **2**. The Fe–OP distances are equal, and the Fe–N distances (2.171–2.177 Å) are effectively the same. Interestingly, no lengthening of the Fe–N bond trans to the oxo ligand is observed. The corresponding bond lengths in **1** exhibit notably larger deviations. The significant lengthening of the Fe–N distances trans to the bridging oxo ligand for **1** ($Fe–N_{trans}$ = 2.21 Å, $Fe–N_{cis}$ = 2.13 Å) is a feature also observed in the structures of carboxylate-bridged analogues.[10,11a,b]

Table III also compares relevant geometric features of **1**–**3** with EXAFS results for the phosphate derivatives of oxidized uteroferrin (Uf)[8] and beef spleen purple acid phosphatase, BPAP.[2b] A short $Fe–O_{oxo}$ distance (ca. 1.8 Å) has not been observed in the proteins, although other experimental data indicate that it does exist (see below). Note that the Fe···Fe distances in the proteins (3.0–3.2 Å) are shorter than observed for model compounds containing a single hydroxo, alkoxo, or phenoxo diiron(III) bridge (Fe···Fe = 3.4–3.5 Å),[11c,22b] but are very reasonable for the $\{Fe_2O\}^{4+}$ center in doubly- or triply-bridged model compounds (Fe···Fe = 3.1–3.3 Å).[10,11a,b,22a] It is also interesting that the Fe–O–Fe angles calculated from the Fe–O and Fe···Fe distances given for the acid phosphatases (∠Fe–O–Fe = 100–110°) are unrealistically small, suggesting that either the reported Fe···Fe distances are too short or the Fe–O distances too long. Such diminished Fe–O–Fe angles have been observed in model compounds containing two monodentate (e.g., hydroxo, phenoxo, alkoxo) bridging ligands,[23] and it is possible that the protein diiron centers have a similar structure.

(22) (a) Yan, S.; Que, L., Jr.; Taylor, L. F.; Anderson, O. P. *J. Am. Chem. Soc.* **1988**, *110*, 5222–5224. (b) Murch, B. P.; Bradley, F. L.; Que, L., Jr. *J. Am. Chem. Soc.* **1986**, *108*, 5027–5028. (c) Wieghardt, K.; Pohl, K.; Gebert, W. *Angew. Chem., Int. Ed. Engl.* **1983**, *22*, 727–728. (d) Chaudhuri, P.; Wieghardt, K.; Nuber, B.; Weiss, J. *Angew. Chem., Int. Ed. Engl.* **1985**, *24*, 778–779. (e) Toftlund, H.; Murray, K. S.; Zwack, P. R.; Taylor, L. F.; Anderson, O. P. *J. Chem. Soc., Chem. Commun.* **1986**, 191–193. (f) Gomez-Romero, P.; Casan-Pastor, N.; Ben-Hussein, A.; Jameson, G. B. *J. Am. Chem. Soc.* **1988**, *110*, 1988–1990. (g) Vincent, J. B.; Huffman, J. C.; Christou, G.; Li, Q.; Nanny, M. A.; Hendrickson, D. N.; Fong, R. N.; Fish, R. H. *J. Am. Chem. Soc.* **1988**, *110*, 6898–6900. (h) Yan, S.; Cox, D. D.; Pearce, L. L.; Juarez-Garcia, C.; Que, L., Jr.; Zhang, J. H.; O'Connor, C. J. *Inorg. Chem.* **1989**, *28*, 2507–2509.

(23) (a) Murch, B. P.; Bradley, F. L.; Boyle, P. D.; Papaefthymiou, V.; Que, L., Jr. *J. Am. Chem. Soc.* **1987**, *109*, 7993–8003. (b) Chiari, B.; Piovesana, O.; Tarantelli, T.; Zanazzi, P. F. *Inorg. Chem.* **1984**, *23*, 3398–3404. (c) Chiari, B.; Piovesana, O.; Tarantelli, T.; Zanazzi, P. F. *Inorg. Chem.* **1983**, *22*, 2781–2784. (d) Ou, C. C.; Lalancette, R. A.; Potenza, J. A.; Schugar, H. J. *J. Am. Chem. Soc.* **1978**, *100*, 2053–2057. (e) Thich, J. A.; Ou, C. C.; Powers, D.; Vasiliou, B.; Mastropaolo, D.; Potenza, J. A.; Schugar, H. J. *J. Am. Chem. Soc.* **1976**, *98*, 1425–1433.

Table IV. Comparison and Assignment of Electronic Transitions of $[Fe_2O\{O_2P(OC_6H_5)_2\}_2(HBpz_3)_2]$, **1**, $[Fe_2O\{O_2P(C_6H_5)_2\}_2(HBpz_3)_2]$, **2**, and $[Fe_2O(O_2CCH_3)_2(HBpz_3)_2]$, **3**

1		2		3[a]		
λ, nm	ε, M^{-1} cm^{-1}/Fe	λ, nm	ε, M^{-1} cm^{-1}/Fe	λ, nm	ε, M^{-1} cm^{-1}/Fe	assignment[b]
263 sh[c]	~4200	265[d]	4600	262	3380	LMCT
320	5150	317	3680	339	4635	LMCT[e]
366	4630	361	3160	358 sh		LMCT[e]
				~400[f]	<200	$O^{2-} \rightarrow$ FeCT[g]
445 sh	~400	442 sh	278	457	505	$^6A_1 \rightarrow [^4T_2](^4D)$[h]
485 sh	228	479	205	492	460	$^6A_1 \rightarrow [^4A_1,^4E](^4G)$[h]
~500[i]	<50	519 sh	73	528 sh		$O^{2-} \rightarrow$ FeCT[g]
625	64	623	60	695	70	$^6A_1 \rightarrow [^4T_2](^4G)$[j]
1005	4.4	940	3.3	995	3.5	$^6A_1 \rightarrow [^4T_1](^4G)$[j]

[a] Reference 10. [b] Based on ideal octahedral symmetry. [c] Fine structure at 253 and 270 nm. [d] Fine structure at 259 and 272 nm. [e] Includes $O^{2-} \rightarrow$ Fe CT (ref 24a). [f] From excitation profile, ref 24b. [g] Reference 24. [h] Reference 24a. [i] From excitation profile. [j] References 10, 11b, and 24.

The Fe···P distances in the proteins are unfortunately not very indicative of the structure of the core. They are consistent with either bridging or terminal phosphate coordination.

Electronic and Vibrational Spectroscopy. The optical spectra of **1** and **2** in CH_2Cl_2 are shown in Figure 2, and Table IV contains a listing of electronic transitions and their assignments for **1**, **2**, and **3**. Many features characteristic of the dicarboxylate-bridged (μ-oxo)diiron(III) core[10,11a,b] are also present in the phosphate-bridged complexes, since absorption energies and intensities compare well for the two classes of compounds. The spectra are dominated by ligand → Fe(III) charge-transfer transitions in the ultraviolet and ligand field transitions in the visible and near-infrared regions.[10,11b,24] It has been shown that features in oxo-bridged diiron(III) complexes between 235 and 275 nm can arise from a carboxylate → Fe charge-transfer transition.[24a] The existence of such bands is not diagnostic of carboxylate coordination, however, since similar bands are observed for the phosphate-bridged complexes **1** and **2** as well as for compounds such as $FeCl_3$, $(Et_4N)[FeCl_4]$, $(Et_4N)_2[Fe_2OCl_6]$,[19] and $[Fe(HBpz_3)_2](ClO_4)$ in CH_2Cl_2 or CH_3CN.[25] It appears that various ligand → Fe(III) charge-transfer bands can occur in this region. Two absorptions falling between 400 and 300 nm have been assigned to charge-transfer bands arising from the oxo bridge.[11b,24a] These bands also may result from a combination of different ligand → Fe(III) charge-transfer transitions, since similar bands have been observed in mononuclear ferric complexes.[25] Interestingly, the intensities of these transitions are higher in **1** (4600–5200 cm^{-1} M^{-1}) than in other oxo-bridged compounds and proteins, including **2**.[10,11b] Transitions observed between 550 and 400 nm for **1** and **2** are only about half as intense as for carboxylate-bridged analogues, and they are less well resolved. These features were identified as ligand field transitions in the carboxylate-bridged complexes and proteins,[24a] as were the two bands in the 550–1100 nm region.[11b,24a,b] These normally forbidden ligand field transitions are quite intense (3–600 cm^{-1} M^{-1}), because the two iron atoms are antiferromagnetically coupled, relaxing the usual spin restrictions.[24a] By comparison of the positions of the ligand field transitions of **1**, **2**, and **3**[10] and from inspection of the Tanabe–Sugano diagram for a high-spin d^5 system,[26] it appears that diphenylphosphinate provides a slightly weaker field than diphenyl phosphate and that they both create weaker fields than carboxylates. The 940-nm transition for **2** occurs at slightly higher energy than measured for any of the oxo-bridged diiron(III) proteins or model compounds studied so far. The weak shoulder observed at 517 nm for **2** may well correspond to an oxo → Fe(III) charge-transfer transition (see below).

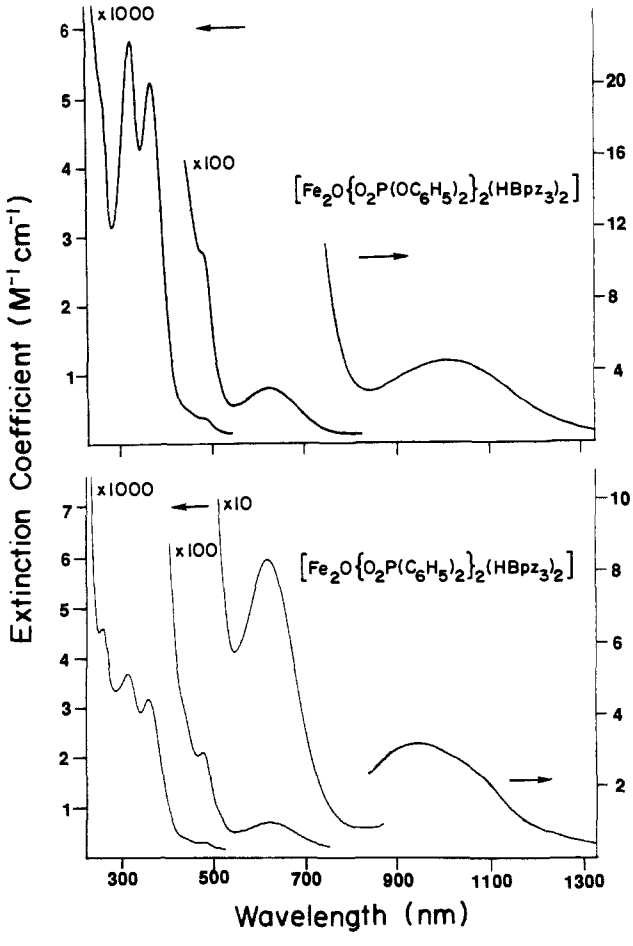

Figure 2. Optical spectra of $[Fe_2O\{O_2P(OC_6H_5)_2\}_2(HBpz_3)_2]$, **1**, and $[Fe_2O\{O_2P(C_6H_5)_2\}_2(HBpz_3)_2]$, **2**, in CH_2Cl_2 solution.

Unfortunately, the optical spectra of oxidized uteroferrin and beef spleen PAP are dominated by peptide absorptions and the tyrosinate-to-iron charge-transfer transition (ca. 550 nm).[8] There are many similarities between these spectra and those of **1**, **2**, and **3**, however. Both proteins have a pronounced shoulder at ca. 320 nm,[2d,3d] and several features are observed for oxidized uteroferrin between 250 and 290 nm.[3d] There is also evidence that a band at 550 nm in Uf_o has a contribution from a transition near 475 nm.[3d] These results suggest that it might be possible to subtract the phenolate-to-metal charge-transfer band from the visible spectra of the proteins and to compare the resulting features with characteristic bands of the $[Fe_2O(O_2XR)_2]^{2+}$ center, where RXO_2^- is carboxylate or phosphate, in the 400–550-nm or 600–700-nm regions. Near-IR spectra of the proteins, if obtainable, would also be very helpful in determining the structure of the diiron center of beef spleen purple acid phosphatase and of uteroferrin.

The resonance Raman spectrum of **1** at 457.9-nm excitation is shown in Figure 3. To confirm assignment of lines corresponding to vibrations of the (μ-oxo)diiron(III) unit, the spectrum of ^{18}O-enriched **1** was recorded (Figure 3, bottom panel). Two features shift upon isotopic substitution. The line at 478 cm^{-1} moves to 464 cm^{-1} after ^{18}O exchange and is assigned to the symmetric Fe–O–Fe stretch, ν_s, which is expected to occur in this region. We assign the second shifting feature, which moves from 950 to 927 cm^{-1} upon ^{18}O substitution, to the first overtone of the symmetric Fe–O–Fe stretch, $2\nu_s$. Changes also occur in the spectrum close to the solvent band at 742 cm^{-1}, which may be caused by the asymmetric Fe–O–Fe stretch, ν_{as}. The Raman spectrum of **2** is dominated by a band at 485 cm^{-1}, assigned to the Fe–O–Fe

(24) (a) Reem, R. C.; McCormick, J. M.; Richardson, D. E.; Devlin, F. J.; Stephens, P. J.; Musselman, R. L.; Solomon, E. I. *J. Am. Chem. Soc.* **1989**, *111*, 4688–4704. (b) Sanders-Loehr, J.; Wheeler, W. D.; Shiemke, A. K.; Averill, B. A.; Loehr, T. M. *J. Am. Chem. Soc.* **1989**, *111*, 8084–8093. (c) Czernuszewicz, R. S.; Sheats, J. E.; Spiro, T. G. *Inorg. Chem.* **1987**, *25*, 2063–2067.

(25) Turowski, P. N.; Micklitz, W.; Armstrong, W. H.; Lippard, S. J. Unpublished results.

(26) Figgis, B. N. *Introduction to Ligand Fields*; John Wiley & Sons: New York, 1966; p 163.

Table V. Comparison of Bond Angles and Stretching Frequencies of the Fe–O–Fe Interaction in Bridged Dinuclear Complexes

complex	∠Fe–O–Fe, deg	ν_s[a], cm^{-1}	∠Fe–O–Fe[b] (calcd), deg	ν_s (calcd),[b] cm^{-1}
1. $[Fe_2O(O_2CCH_3)_2(tacn)_2]I_2$[c]	118.7	540	118.2	538
2. $[Fe_2O(O_2CC_6H_5)_2(bzim)_2(ClO_4)_2$[d]	118.7	537	118.9	538
3. $[Fe_2O(O_2CCH_3)_2(metacn)_2](PF_6)_2$[e]	119.7	537	118.9	534
4. $[Fe_2O(O_2CCH_3)_2(tpbn)_2]_2(ClO_4)_4$[f]	121.3	525	121.9	528
5. **3**[g]	123.6	528	121.2	518
6. $[Fe_2O(O_2CCH_3)_2(O3)_2]$[h]	124.4	510	125.7	515
7. $[Fe_2O(O_2CCH_3)(tpa)_2](ClO_4)_3$[i]	129	499	129.9	497
8. $[Fe_2O(O_2CC_6H_5)(hdp)_2](ClO_4)$[j]	129.2	494	128.6	497
9. $[Fe_2O(O_2CC_6H_5)(tpa)_2](ClO_4)_3$[i]	130	497	129.1	495
10. ribonucleotide reductase[k]	130	493	130.1	493
11. **2**	130.6	485	132.2	491
12. **1**	134.7	478	134.1	476
13. azidomethemerythrin[l]	135	507	126.5	475
14. $[Fe_2O\{O_2P(OC_6H_5)_2\}(tpa)_2](ClO_4)_3$[i]	138	454	140.8	463
15. $[(N5)FeOFeCl_3]Cl$[m]	149.8	425	149.9	425
16. $[(N5)FeOFeBr_3]Br$[m]	150.6	422	150.9	423
17. $[Fe_4O_2(OH)_2(mhxta)_2]$[n]	151.2	425	149.9	421
18. $[Fe_2O(H_2O)_2(phen)_4]Cl_4$[o]	155.1	395	162.2	411
19. $(Et_4N)_2[Fe_2OCl_6]$[p]	155.6	458	139.6	410
20. $[Fe_2O(propsal)_4]$[q]	164	403	158.4	392
21. $(enH_2)_2[Fe_2O(hedta)_2]$[r]	165.0	409	155.8	390
22. $[Fe_2O(TPP)_2]$[s]	175.0	363	180	379
23. $[Fe_2O(H_2O)_4(Cl\text{-}pdc)_2]$[t]	180.0	381	172.2	378

[a] ν_s from Raman spectroscopy. For entries 2–4, 7–9, 14–16, and 20–23, ν_s values were obtained from ref 24b. [b] Determined from eq 2 (see text). [c] Tacn = 1,4,7-triazacyclononane, ref 11b and 22c. [d] Bzim = bis(2-benzimidazolylmethyl)amine, ref 22f. [e] Metacn = 1,4,7-trimethyl-1,4,7-triazacyclononane, ref 11c and 22d. [f] Tpbn = tetrakis(2-pyridylmethyl)-1,4-diaminobutane, ref 22e. [g] Reference 10. [h] O3 = (cyclopentadienyl)tris(diethylphosphito-P)cobaltate, ref 11d. [i] Tpa = tris(2-pyridylmethyl)amine, ref 22h and 24b. [j] Hdp = *N*-(*o*-hydroxybenzyl)-*N*,*N*-bis(2-pyridylmethyl)amine, ref 22a. [k] Reference 4. [l] Reference 5. [m] N5 = *N*-hydroxyethyl-*N*,*N*′,*N*′-tris(2-(benzimidazolyl)methyl)-1,2-diaminoethane, ref 28. [n] Mhxta = *N*,*N*′-2-hydroxy-5-methyl-1,3-xylylenebis(*N*-(carboxymethyl)glycine), ref 23a. [o] Phen = 1,10-phenanthroline, ref 29. [p] Reference 19b,c. [q] Propsal = *n*-propylsalicylidineimine, ref 30. [r] Hedta = *N*-hydroxyethyl-1,2-diaminoethane-*N*,*N*′,*N*′-triacetate, en = 1,2-diaminoethane, ref 31. [s] TPP = tetraphenylporphyrin, ref 32. [t] Cl-pdc = 4-chloro-2,6-pyridinedicarboxylate, ref 33.

symmetric stretch. Assignment of the Raman vibrations of **1** and **2** was facilitated by comparison with **3**[10,24c] and with $[Fe_2O(O_2CCH_3)_2(TACN)_2]$,[11b] for which vibrational analyses have been published.

The position of the asymmetric Fe–O–Fe stretch of **1** was revealed by FTIR spectroscopy. The vibration, which shifts from 767 (^{16}O) to 725 cm^{-1} (^{18}O) after isotopic substitution, is hidden under ligand bands but can be identified from the difference spectrum. Another weak feature, which shifts from 475 (^{16}O) to 463 cm^{-1} (^{18}O), may well be the symmetric stretch, since the values correspond with those observed in the Raman spectra for ν_s (Fe–O–Fe). As noted before, the intensity of the asymmetric vibration in these oxo-bridged diiron(III) compounds is very low,[10,11b] such that the asymmetric Fe–O–Fe stretching vibration could not be detected in the IR spectrum of **2**. On the basis of the comparison with similar complexes (see below), this vibration is expected to occur at ca. 764 cm^{-1}, where it would be masked by the strong $HBpz_3^-$ vibration at 756 cm^{-1}. The remaining bands in the infrared and Raman spectra of **1** and **2** consist of the expected vibrations of the coordinated $HBpz_3^-$, $(C_6H_5O)_2PO_2^-$, and $(C_6H_5)_2PO_2^-$ ligands.

By using measured values of ν_s and ν_{as}, the stretch (k_d) and the stretch–stretch interaction (k_{dd}) force constants can be calculated from simplified secular equations derived from a normal mode analysis based on local C_{2v} symmetry.[27] The constants calculated for **1**, k_d = 3.24 mdyn/Å and k_{dd} = 0.46 mdyn/Å, predict values of 464 and 728 cm^{-1} for the symmetric and asymmetric stretching frequencies, respectively, of the ^{18}O-substituted derivative. These values are in good agreement with the experimental ones (464 and 725 cm^{-1}), suggesting that the model used for the calculations is appropriate for this system. Force constants were also calculated for parameters of diiron(III) oxo species compiled by Sanders-Loehr et al.[24b] These force constants generally predict vibrational stretching frequencies for ^{18}O-substituted complexes within 2 cm^{-1} of observed values. When vibrational data for both ^{16}O-oxo- and

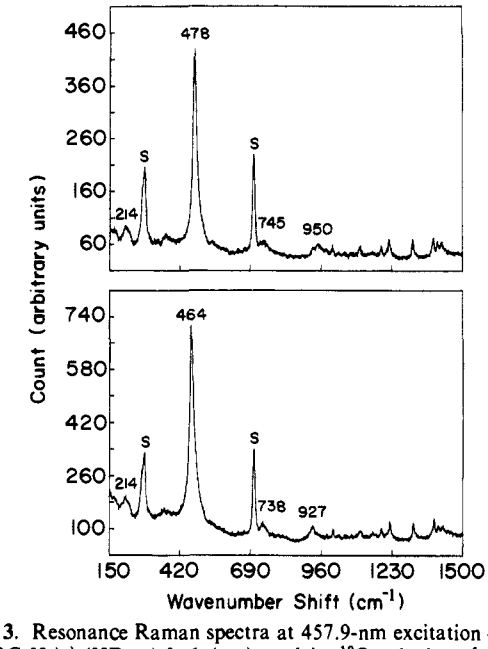

Figure 3. Resonance Raman spectra at 457.9-nm excitation of $[Fe_2O\{O_2P(OC_6H_5)_2\}_2(HBpz_3)_2]$, **1** (top), and its ^{18}O substituted derivative (bottom) in CH_2Cl_2. The peaks labeled S are associated with the solvent.

^{18}O-oxo-bridged diiron(III) complexes are available, the Fe–O–Fe angles may be calculated from the secular equations.[27] Unfortunately, angles calculated in this manner do not agree well with observed ones, commonly deviating by 5–10°.[24b] On the other hand, a good correlation exists between the squares of the vibrational frequencies and the cosines of the Fe–O–Fe angles for (μ-oxo)diiron(III) complexes, as illustrated in Figure 4. A linear expression relating these parameters for ν_s(Fe–O–Fe) is given by eq 2, where ϕ is the Fe–O–Fe angle in deg. Observed and cal-

$$\nu_s^2\ (cm^{-2}) = 4.252 \times 10^5 - 2.826 \times 10^5 \cos \phi \qquad (2)$$

culated values of the Fe–O–Fe angle and ν_s(Fe–O–Fe) for various oxo-bridged diiron(III) complexes are presented in Table V.

(27) (a) Wing, R. M.; Callahan, K. P. *Inorg. Chem.* **1969**, *8*, 871–874. (b) Cotton, F. A.; Wing, R. M. *Inorg. Chem.* **1965**, *4*, 867–873. (c) Nakamoto, K. *Infrared and Raman Spectra of Inorganic and Coordination Compounds*, 4th ed.; John Wiley & Sons: New York, 1986; pp 59–62.

Table VI. Summary of NMR T_1 Values for **1**, **2**, and **3**[a]

	compound					
	1		**2**		**3**[b]	
assignment	shift[c]	T_1, ms	shift, ppm	T_1, ms	shift[c]	T_1, ms
pz (syn, H4 + H5)[d]	13.9	1.6 (3)	14.1, 13.7	1.5 (3)	12.1	2.7 (4)
pz (anti, H4 + H5)[d]	10.9 (sh)	1.6 (3)	11.1, 10.8	1.9 (3)	12.1	2.7 (4)
pz (H3)[d]	~7.9	1.4 (3)	~8.2	0.9 (3)	9.1	0.3 (2)
Ph	7.37	8 (2)	8.49, 7.56	5 (1), 9 (3)		
Ph	7.27	6 (3)	8.12, 7.95	4 (1), 4 (1)	10.5[e]	1.1 (4)[e]
Ph	7.15	12 (1)	7.33, 7.12	8 (1), 8 (2)		
B-H	2.6	0.7 (3)	3.1	0.9 (2)	2.5	1.2 (4)

[a] Shifts are given downfield of TMS. Errors in T_1 values are large because of partial overlaps and many broad proton signals (see Figure 6). [b] Reference 33. [c] Entries are in ppm. [d] See text for diagram of proton positions. [e] Acetate methyl resonance.

Equation 2 was derived from all data in Table V except for those from azidomethemerythrin and $(Et_4N)_2[Fe_2OCl_6]$. The former was omitted because of inherent uncertainties in determining geometric parameters from protein crystallography, and the latter was omitted because it is the only entry for four-coordinate iron and does not fit well on the line. From standard deviations for the complexes in Table V, we estimate the error in angles predicted by eq 2 to be 6° for simple oxo-bridged diiron(III) complexes and 3° for such complexes containing one or two additional bridging ligands. The error in predicting ν_s(Fe–O–Fe) is 12 cm^{-1} in the former case and 6 cm^{-1} in the latter.

The linear relationship between the square of the vibrational frequency and the cosine of the Fe–O–Fe angle for (μ-oxo)diiron(III) complexes is predicted by the secular equations of Wing et al., if all other values remain constant.[27] Since the quantity ($k_d + k_{dd}$) included among these "constants" fluctuates considerably, the correlation is probably fortuitous. Indeed, a similar attempt to correlate asymmetric stretching vibrations to Fe–O–Fe angles resulted in substantial scatter and nonlinearity. A graph in which ν_s and ν_{as} were plotted as a function of the Fe–O–Fe angle was recently reported.[24b] Coincidentally, such a graph also results in a near-linear correlation, especially if only oxo-bridged diiron(III) complexes and proteins containing at least one additional bridge are considered.

The excitation profile from 457.9 to 514.5 nm of the symmetric Fe–O–Fe stretch in the resonance Raman spectrum of **1** was obtained and is shown in Figure 5. A modest peak (30% enhancement) is observed at ~500 nm, and another seems to occur below 450 nm. This excitation profile is similar to those observed for carboxylate-bridged analogues, in which enhancement maxima are reported in two regions, 520–545 and 390–425 nm.[10,11b,24b,c] These maxima were correlated with low intensity oxo → Fe(III) charge-transfer transitions,[24] which sometimes appear as weak shoulders in visible spectra of the complexes.[10,11b,24] Note that the shoulder at 519 nm in the visible spectrum of **2** is close to the weak enhancement observed at ~500 nm in the excitation profile of **1** (see Table IV).

The symmetric Fe–O–Fe stretching vibration has not been observed in the Raman spectra of uteroferrin or beef spleen phosphatase, despite efforts to find it.[2a,c,8] Perhaps the 521-cm^{-1} peak in oxidized BPAP, assigned to the Fe(III) tyrosinate chromophore with contribution from a bridging ligand,[2a] coincides with ν_s(Fe–O–Fe). The excitation profile of this vibration appears to be dominated by the Fe(III) tyrosinate mode.[2a] Since shifts in the presence of $H_2{}^{18}O$ or D_2O are not observed,[2a] the diiron(III) center is probably not accessible to solvent. A similar feature was observed in oxidized uteroferrin.[2a] A symmetric stretch at 521 cm^{-1} would, according to eq 2, correspond to an Fe–O–Fe angle of 123 (3)°, a very reasonable value. Neighboring ligands, especially those trans to the oxo bridge, may affect the intensity of the vibration.[24b] Studies on **1** and **2** show that coordination of phosphate versus carboxylate ligands cis to the oxo bridge does not significantly decrease the intensity of the symmetric Fe–O–Fe stretch.

Electrochemistry. Cyclic voltammograms of **1** and **2** were obtained, and both compounds were found to undergo irreversible reductions, forming $[Fe(HBpz_3)_2]^+$. The reduction of **2** occurs at −0.67 V vs SCE, a value somewhat more favored than for

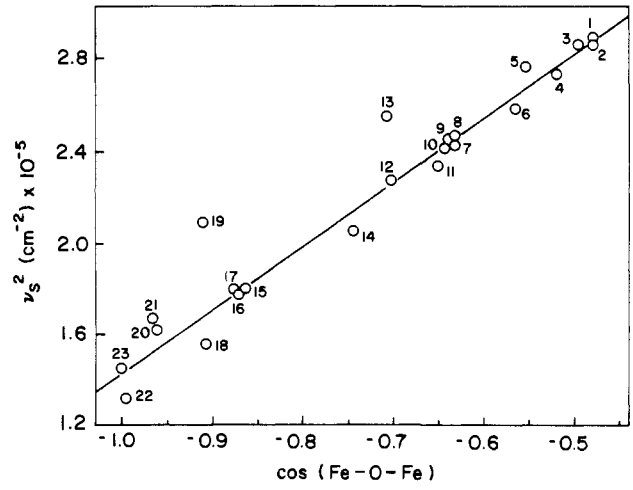

Figure 4. Plot of the square of symmetric stretching frequencies versus the cosine of Fe–O–Fe angles of complexes listed in Table V.

reduction of **3** (−0.71 V).[10] Reduction of **1** occurs at −1.00 V vs SCE. In both samples the $[Fe(HBpz_3)_2]^+/[Fe(HBpz_3)_2]$ couple that appears is reversible, with a half-wave potential of +0.23 V vs SCE and a peak-to-peak separation of 59 mV. Thus, neither **1** nor **2** displays the reversible redox properties of dinuclear iron containing proteins. Although **1** and **2** are fairly similar to **3** in other respects, the positions of their reduction waves are rather different, implying that small changes in the ligand environment can have a large effect on redox potentials.

Mössbauer Spectra. The ^{57}Fe Mössbauer spectra of **1** and **2** were obtained at 4.2 and 80 K. The parameters are compared with those of purple acid phosphatases and carboxylate-bridged model compounds in Table III. The parameters of **1** and **2** are representative of oxo-bridged diiron(III) complexes and proteins in general (ΔE_Q = 1.5–2.1 mm/s, δ = 0.45–0.95 mm/s).[11a,34] In contrast, the quadrupole splitting values for the two iron sites in the phosphate-bound forms of oxidized uteroferrin and beef spleen phosphatase are rather unusual.[2a,3a] The values appear to be too low for an oxo-bridged structure but too high for a hydroxo-bridged or mononuclear structure (ΔE_Q < 0.6 mm/s). A few singly-bridged diiron(III) oxo complexes with quadrupolar splitting parameters of less than 1.1 mm/s are known, however.[34] Possibly, the bridging oxo ligand in the phosphatases is involved in hydrogen bonding, or there is an anion, probably inorganic phosphate, cis

(28) Gomez-Romero, P.; DeFotis, G. C.; Jameson, G. B. *J. Am. Chem. Soc.* **1986**, *108*, 851–853.
(29) Plowman, J. E.; Loehr, T. M.; Schauer, C. K.; Anderson, O. P. *Inorg. Chem.* **1984**, *23*, 3553–3559.
(30) Davies, J. E.; Gatehouse, B. M. *Cryst. Struct. Commun.* **1972**, *1*, 115–120.
(31) (a) Lippard, S. J.; Schugar, H. J.; Walling, C. *Inorg. Chem.* **1967**, *6*, 1825–1831. (b) Schugar, H. J.; Rossman, G. R.; Barraclough, C. G.; Gray, H. B. *J. Am. Chem. Soc.* **1972**, *94*, 2683–2690.
(32) Hoffman, A. B.; Collins, D. M.; Day, V. W.; Fleischer, E. B.; Srivastava, T. S.; Hoard, J. L. *J. Am. Chem. Soc.* **1972**, *94*, 3420–3426.
(33) Ou, C. C.; Wollmann, R. G.; Hendrickson, D. N.; Potenza, J. A.; Schugar, H. J. *J. Am. Chem. Soc.* **1978**, *100*, 4717–4724.
(34) Murray, K. S. *Coord. Chem. Rev.* **1974**, *12*, 1–35.

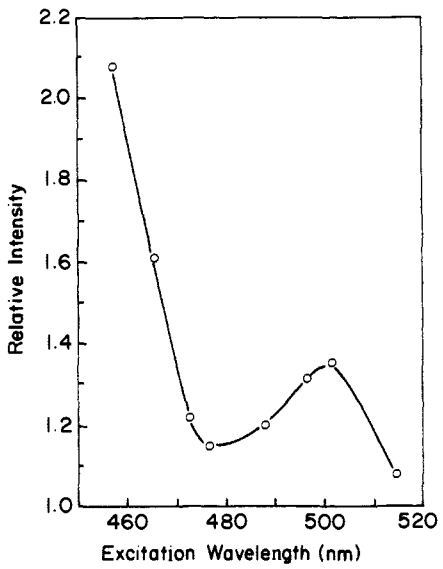

Figure 5. Excitation profile of the 478-cm^{-1} Raman band (ν_s Fe–O–Fe) of $[Fe_2O\{O_2P(OC_6H_5)_2\}_2(HBpz_3)_2]$, **1**, from 457.9 to 514.5 nm.

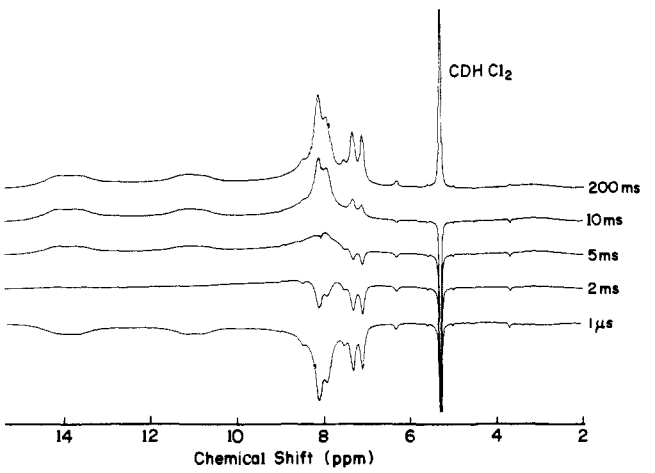

Figure 6. Proton NMR spectra of $[Fe_2O\{O_2P(C_6H_5)_2\}_2(HBpz_3)_2]$, **2**, in CH_2Cl_2 using varying relaxation delay times, as indicated.

to the oxo ligand, which lessens the magnitude of the electric field gradient imposed by the short Fe–O–Fe bond, thus, inducing smaller quadrupolar splitting. The quadrupole splitting values of the two iron atoms in oxidized uteroferrin without bound phosphate (ΔE_Q = 1.65, 2.12 mm/s) fall in the normal range for oxo-bridged diiron(III) complexes.[3c,8]

NMR Spectra. The ^1H NMR spectra of **1** and **2** are typical of strongly coupled, high-spin diiron(III) complexes.[10] Assignments of the resonances, summarized in Table VI, were made by comparison with the spectrum of **3**[10] and by NMR T_1 measurements. The ^1H NMR spectrum of **2** at different relaxation delay times is presented in Figure 6. As can be seen in Table VI, protons closer to the diiron(III) centers relax more rapidly than those farther away. A similar phenomenon was observed for **3**.[35] The $\{Fe_2O\}^{4+}$ units decrease spin–lattice relaxation times by factors ranging from two for the solvent to as much as 100 for protons closest to the dinuclear iron centers. Only downfield shifts from free ligand values were observed. Resonances of protons on the hydrotris(1-pyrazolyl)borate ligands are the most shifted and broadened. These resonances are very similar in **1**, **2**, and **3** (see Table VI). The B–H resonances of **1** and **2** occur at 2.5 and 2.9 ppm, with spin–lattice relaxation times of 0.9 and 1.3 ms, respectively. These resonances are only slightly downfield from those of the free ligand at 2.23 ppm. The pyrazole proton resonances exhibit relaxation times of 0.5–3 ms. Six pyrazole proton resonances are expected, since the three unique protons of the pyrazole rings trans to the oxo bridge are in a different chemical environment than those of the rings in cis positions. The pyrazole resonances of **2** are narrower and much better resolved than those of **1**, such that inequivalences in the chemical shifts of the latter cannot be clearly delineated. Resonances of protons in the 4- and 5-positions probably experience similar shifts to one another, since both are about the same distance from the iron atoms. The resonances at ~13.9 ppm in **1** and **2** are approximately twice as

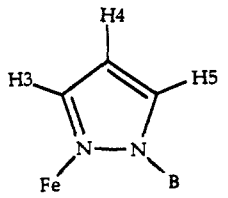

intense as those at ~10.9 ppm, allowing the pyrazole ring proton assignments to be made in the following manner. The peak at 13.9 ppm in the spectrum of **1** and the peaks at 13.7 and 14.1 ppm in **2** are assigned to protons in the 4- and 5-positions of the *cis*-pyrazole rings, corresponding to a 6–7-ppm shift from free ligand values. The signals of the trans H4 and H5 protons (Table VI) are shifted by 4–5 ppm. The resonances of the H3 protons lie under the phenyl resonances, as is evident upon close examination of the phenyl proton spectral region. Positions of the H3 resonances were determined from spectra obtained by using a relaxation delay time of ~3 ms, such that the spins of the pyrazole protons have relaxed but not those of the phenyl protons. The resonances occur at 7.9 ppm for **1** and 8.2 ppm for **2**, being shifted by only ~0.5 ppm from the free ligand values. These results are similar to those obtained for **3**. The phenyl protons of the diphenyl phosphate or diphenylphosphinate ligands are much farther removed from the iron atoms and consequently are neither broadened nor shifted as much as the pyrazole ring protons. The expected complex multiplets are broadened beyond recognition. Three phenyl resonances are observed in the spectrum of **1** at 7.37, 7.27, and 7.15 ppm, with relaxation times of 9–12 ms. The six phenyl resonances in **2** have slightly shorter relaxation times, because the protons are nearer to the iron atoms.

The ^1H NMR spectra of oxidized uteroferrin and beef spleen phosphatase have not yielded any information on the structure of the dinuclear iron center, since no signals were observed outside the protein envelope (0–10 ppm).[8] Such spectra are consistent with a strongly antiferromagnetically coupled diiron core in the proteins, such as exists in oxo-bridged diiron(III) units (see below). In such a case, it may be possible in the future to observe signals for histidine ligands, if present, at ~10–20 ppm in the ^1H NMR spectra of the proteins. If the magnitude of the antiferromagnetic exchange coupling constant were below ~100 cm^{-1}, ligand residues would be more shifted and thus visible outside the protein envelope.

^{31}P NMR spectra of **1** and **2** were obtained, but a phosphorus signal was not observed (after 16000 scans), suggesting that the nuclear spin relaxes too quickly to be detected. Phosphate-bound oxidized uteroferrin does not have an observable ^{31}P NMR signal either, possibly because the site has a large amount of chemical shift anisotropy.[3a]

Magnetic Susceptibility. Results of magnetic susceptibility measurements for a powdered sample of **1** are shown in Figure 7. The data of **1** were well fit for an antiferromagnetic coupling constant, J, of −97.5 (1) cm^{-1} and a paramagnetic impurity term, p, of 4.7(7) × 10^{-5}, with a spin-exchange Hamiltonian, $\mathcal{H} = -2JS_1 \cdot S_2$.[11a,18] The best fit for **2** included a Weiss parameter, θ, associated with the paramagnetic impurity, and the results were J = −93 (1) cm^{-1}, p = 1.67 (5) × 10^{-2}, and θ = −11.2 (1). The large negative θ term necessary to obtain fits to the data in two separate studies of **2** may be explained by a polymeric iron phosphate impurity which appears to form during recrystallizations of **2**. A similar θ term was previously observed in magnetic studies of $[Fe_2O(OAc)_2(Me_3TACN)_2](PF_6)_2$, where Me_3TACN is 1,4,7-trimethyl-1,4,7-triazacyclononane.[11a] The antiferromagnetic exchange interaction constants indicate strong coupling in the oxo-bridged diiron centers. The values are somewhat less negative

(35) Beer, R. H.; Lippard, S. J. Unpublished results.

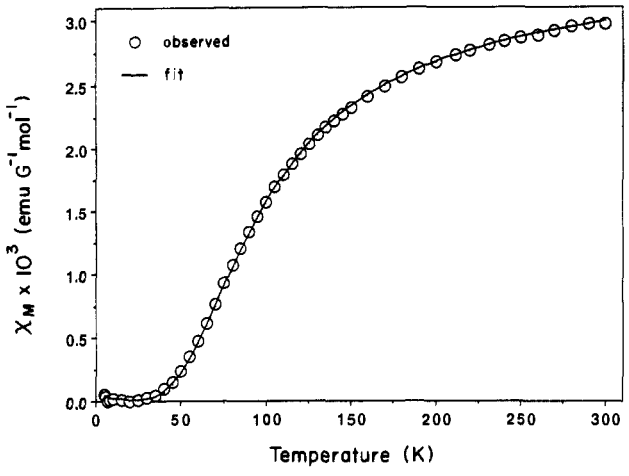

Figure 7. Plot of magnetic susceptibility versus temperature for solid $[Fe_2O\{O_2P(OC_6H_5)_2\}_2(HBpz_3)_2]\cdot CHCl_3$, **1**·$CHCl_3$.

than found for **3** ($J = -121$ cm^{-1}),[10] probably owing to the slightly increased Fe–O_{oxo} distances in **1** and **2**. For diiron(III) compounds and larger iron oxo aggregates which are bridged by two or more ligands, a correlation (eq 3) between the coupling constant and

$$-J\ (\text{cm}^{-1}) = 8.763 \times 10^{11} \exp(-12.663P) \qquad (3)$$

the coupling distance (P, Å) has been observed.[36] No correlation between $-J$ and the Fe–O–Fe angle was observed in this study.[36b] In the complexes discussed here, P is equal to the average Fe–O_{oxo} distance. For the Fe–O_{oxo} distances of **1** and **2**, 1.808 and 1.812 Å, expected J values of −99.9 and −95.0 cm^{-1}, respectively, can be calculated from the expression correlating the parameters[36b] in agreement with the experimentally determined values, −97.5 and −93 cm^{-1}. If the same correlation is used to estimate the coupling constants of uteroferrin and beef spleen phosphatase from the Fe–O distances of 1.96 and 1.98 Å, respectively, the results ($J \sim -15$ and −11 cm^{-1}) are very different from the experimentally obtained values of $-J > 40$ and $-J > 150$ cm^{-1}, respectively.[2b,8] The low calculated coupling constants seem inconsistent with the NMR results for Uf (see above), since weakly coupled diiron(III) centers exhibit characteristic strongly shifted NMR signals.[11c] Alternatively, the Uf resonances may simply be too broad to be observable. If the measured antiferromagnetic coupling constants are used to calculate distances, Fe–O bond lengths of less than 1.88 Å for Uf and of less than 1.78 Å for BPAP are obtained. These values are entirely consistent with an oxo-bridged formulation. Since a sulfido bridge does not appear to be present in purple acid phosphatases on the basis of spectroscopic results,[2,3,8] the high experimentally obtained coupling constants can best be explained by the presence of an oxo bridge.[8]

The effective magnetic moments per iron of **1** and **2** in the solid state, 1.87 and 1.97 μ_B at 295 and 290 K, respectively, agree with the values of 1.91 and 1.98 μ_B measured for **1** and **2** in CD_2Cl_2 solution with use of an NMR method,[16] consistent with retention of the oxo-bridged structure for both complexes in solution.

(36) (a) Gorun, S. M.; Lippard, S. J. *Recl. Trav. Chim. Pays-Bas* **1987**, *106*, 417. (b) Gorun, S. M.; Lippard, S. J. Submitted for publication.

Conclusions

Complexes containing a phosphate-bridged (μ-oxo)diiron(III) core, such as may exist in the metalloproteins uteroferrin and beef spleen purple acid phosphatase, have been prepared. The core in these complexes is expanded relative to μ-oxo-di-μ-carboxylato complexes, decreasing the magnitude of the antiferromagnetic spin exchange coupling constants and affording larger paramagnetic shifts in the ^{1}H NMR spectra of the phosphate-bridged complexes. The enlarged Fe–O–Fe angles in the complexes lower the frequencies of the symmetric stretching vibrations of the Fe–O–Fe unit. These results further demonstrate the potential for the magnetic and vibrational parameters of iron oxo proteins to afford useful information about the geometry of their cores. Electronic transitions are similar for the phosphate-bridged complexes and their carboxylate-bridged analogues. Shifts occur in the d–d transitions which imply that diphenyl phosphates and diphenylphosphinates are weaker field ligands than carboxylates. Mössbauer parameters are only slightly affected by replacement of phosphate for carboxylate bridges and the consequent structural changes. The electrochemical potentials of the irreversible reductions of the complexes are, however, influenced by bridging ligand substitution.

Phosphate ligands have been implicated in the unusual magnetic and spectroscopic properties of uteroferrin and beef spleen purple acid phosphatase. The diphenyl phosphate- and diphenylphosphinate-bridged complexes **1** and **2** do not exhibit these unusual properties, so that a similar oxo-bridged phosphate-bridged diiron(III) structure is unlikely to occur in the proteins. The model complexes do not explain why a symmetric Fe–O–Fe vibration cannot unambiguously be identified in the Raman spectra of the proteins, nor why the EXAFS results of the proteins are inconsistent with the presence of an oxo bridge. As in the phosphatases, however, no signals were observed in the ^{31}P NMR spectra of the model compounds. The lack of ^{31}P signals therefore does not constitute hard evidence that phosphate ligands are not present in purple acid phosphatases.

Acknowledgment. This work was supported by the National Institutes of Health Grant GM-32134 from the National Institutes of General Medical Sciences. P.N.T. and W.H.A. gratefully acknowledge support under Training Grant CA-09112, respectively, and M.E.R. thanks the National Science Foundation for a predoctoral fellowship. We thank Dr. G. C. Papaefthymiou for obtaining Mössbauer spectra and for assistance with the magnetic susceptibility measurements and Drs. K. J. Ahmed and J. G. Bentsen for assistance with the electrochemical and Raman studies, respectively. Additionally, we appreciate the help of R. H. Beer and Dr. S. G. Bott, and we thank Dr. J. Sanders-Loehr for kindly supplying a preprint of ref 24b and a referee for several helpful comments.

Registry No. $[Fe_2O\{O_2P(OC_6H_5)_2\}(HBpz_3)_2]$, 96502-34-0; $[Fe_2O\{O_2P(C_6H_5)_2\}_2(HBpz_3)_2]$, 124042-43-9; $HO_2P(OC_6H_5)_2$, 838-85-7; $[Fe_2O(O_2CCH_3)_2(HBpz_3)_2]$, 86177-70-0; Fe, 7439-89-6; O_2, 7782-44-7; diphenylphosphinic acid, 1707-03-5.

Supplementary Material Available: Tables S3–S8 of non-hydrogen atomic thermal parameters, atomic positional parameters, and all bond distances and angles for **1** and **2** (14 pages); Tables S1 and S2 of observed and calculated structure factors (83 pages). Ordering information is given on any current masthead page.